RMetS

Royal Meteorological Society

Composite life cycle of tropical mesoscale convective systems from geostationary and low Earth orbit satellite observations: method and sampling considerations

Thomas Fiolleau[a] and Rémy Roca[b]*

[a]*Laboratoire de Météorologie Dynamique, IPSL/CNRS, Paris, France*
[b]*Laboratoire d'Etudes en Géophysique et Océanographie Spatiales, Toulouse, France*

*Correspondence to: R. Roca, LEGOS/OMP, 14 avenue Edouard Belin, 31014 Toulouse, France.
E-mail: roca@legos.obs-mip.fr*

The ability of the current and upcoming space-borne microwave observing systems to document precipitation processes during the life cycle of tropical convective systems is investigated with emphasis on sampling considerations. A composite technique is introduced that will serve as a Day 1 algorithm for the Megha-Tropiques mission. It is exemplified using the Tropical Rainfall Measurement Mission (TRMM) satellite observations from the TRMM Microwave Imager (TMI) instrument and the fleet of operational geostationary infrared images for the boreal summer 2009 over the whole intertropical belt. At the system scale, over both land and oceanic regions, rainfall is overall strong at the beginning (the first third) of the life cycle and then smoothly decreases as the system shrinks and dissipates. Larger rain yields are observed for the land systems ($\sim$6 mm h^{-1} maximum) compared to the systems over ocean ($\sim$4 mm h^{-1} maximum). An in-depth analysis of the sensitivity of the results to various aspects of the sampling is performed using simulated observations. The benefit of using various platforms is discussed, including considerations of constellation configuration. The entire Tropics as well as regional scales are explored, revealing the expected improvements from the inclusion of the Megha-Tropiques observations. The sampling results are also strongly supportive of the use of multiple-platform microwave observations from the upcoming Global Precipitation Mission constellation to build a mesoscale convective system precipitation composite life cycle, although the merging of the parameters derived from various resolution radiometers would deserve further investigations. Copyright © 2013 Royal Meteorological Society

1. Introduction

Deep convective cloud systems play a major role in the tropical climate by connecting the low atmospheric levels to the free troposphere, through the vertical transport of mass, water and momentum. The resulting vertical distribution of associated cumulus-induced heating, cloud radiative cooling and momentum flux strongly influences the energy and water cycle and the large-scale circulation (Roca *et al.*, 2010). The vertical profile of net heating and of momentum flux due to these mesoscale convective systems (MCSs) is driven by the relative contribution

of the convective and stratiform processes to the whole cloud system (Houze, 2004). The convective/stratiform fraction within a cloud system hence determines to a large extent its effect on its environment. It further provides the physical link between the internal system dynamics and the impact on its larger-scale environment. The stratiform region is composed of cloud material originating from previously active deep convective cells and therefore is of utmost importance to the understanding of the evolution in time of the broad precipitating characteristics of the mesoscale convective system during its life cycle and the convective/stratiform fraction in particular. While the geostationary infrared (IR) observations are an invaluable source of information to describe the morphology of the cold cloud shield of the MCS along it life cycle, it falls short as far as the quantitative investigation of the precipitation and microphysical processes and the internal dynamics of the storms are concerned (e.g. Liu *et al.*, 2007). One way to overcome the limits of the geostationary IR is then to combine these morphological parameters with existing exogenous geophysical relevant products.

At the structural level, in a *static* framework, a number of studies have investigated the scale dependence of the IR-derived clusters using various ground-based observations (see Houze and Betts, 1981; Yuter and Houze, 1998) feeding our understanding of the processes underlying anvil formation and maintenance (Houze, 2004). More recently, efforts have been geared towards taking advantage of the active instruments on board the TRMM satellite to investigate the rain and microphysical structural properties of the MCS anvil clusters (e.g. Nessbitt *et al.*, 2006; Cetrone and Houze, 2009). Using a refined cloud cluster detection technique, Yuan and Houze (2010) explored, using Cloudsat, microphysical profiles as a function of the morphological characteristics of IR-derived cold clusters. This study revealed that the most frequent anvil thickness is 4−5 km and that thicker anvils are mainly associated with oceanic systems, indicative of anvil spread from the primary raining part of the storms.

At the life cycle level, in a *dynamic* framework, many fewer multi-observational studies have been performed. Again radar measurements obtained during observing campaigns have helped a lot in understanding the life cycle of the cold cloud shield of the MCS (Houze, 1982; Williams and Houze, 1987; Diongue *et al.*, 2002; Machado and Laurent, 2004). Beyond individual campaigns, such data fusion approaches have been successfully implemented taking benefit of surface rainfall observations networks. Based on compositing techniques, such investigation revealed, for instance, key features of the precipitation life cycle of mesoscale convective complexes over central USA (e.g. McAnelly and Cotton, 1989). More recently, these compositing efforts have been extended to the fusion of observations from low Earth-orbiting satellites together with the life cycle morphology of the MCS derived from geostationary IR data, over large and oceanic domains, overcoming the limitations induced by the use of regional ground-based observing systems. Kondo *et al.* (2006) investigated the Maritime Continent and Western Pacific area. Their study indicates that strong system-average rain rates are observed in the first stages of MCS development, followed by a gradual decrease, and that convective rain fraction, derived from the TRMM precipitation radar, behaves similarly. Inoue *et al.* (2009), on the other hand, focus on the Eastern Pacific region and

suggest that the early-stage enhanced rain rates are linked to smaller occurrence of cirrus clouds compared to the termination stage of the MCS life cycles. Futyan and Del Genio (2007) compiled METEOSAT Second Generation Geostationary Earth Radiation Budget measurements using the Detect and Spread technique (Boer and Ramanathan, 1997) and an overlap tracking approach into composite life cycles of MCSs over Africa and the Atlantic Ocean region. They further made use of the TRMM radar observations to investigate the internal dynamics of the MCS during the time evolution of its life cycle thanks to a dedicated compositing technique. Their results suggest drastic differences of the MCS life cycles between the Atlantic Ocean and the West African region. Unlike the latter, the former systems show a steady convective rain fraction along their life cycles. These recent studies are refining our conceptual models of the life cycle of organized convection over various regions of the Tropics (e.g. Liu *et al.*, 2007, Figure 12) and are useful to confront the simulation of cloud-resolving models (Futyan and Del Genio, 2007; Del Genio, 2012) as well as for guiding the development of a new parametrization of convection for climate models (Grandpeix and Lafore, 2010; Pritchard *et al.*, 2011).

In this paper, a compositing technique is introduced that merges the MCS morphological parameters derived from the geostationary infrared imagery together with the observations from low earth-orbiting platforms during the life cycle of the storms. The technique and its results will form the core of the operational algorithm (Day 1) for the Megha-Tropiques mission (Roca *et al.*, 2010) and is intended to be applied systematically over the whole intertropical belt during the multi-year lifespan of the mission. In this paper, the theoretical bases of this algorithm are presented. The geophysical products are exemplified for the summer 2009 period, using the TMI/TRMM observations and the infrared data from the fleet of geostationary satellites operating at that time, providing for the first time a composite analysis for the whole intertropical belt. Sensitivity analysis of the composites to sampling by microwave measurements is then performed using simulated observations of the Megha-Tropiques radiometer, as well as idealized configurations of microwave imagers' constellations prefiguring the Global Precipitation Mission (Hou *et al.*, 2008). A summary and perspectives section end the paper.

2. Data and products

2.1. Geostationary infrared observations

In summer 2009 the monitoring of the whole intertropical belt was achieved thanks to the use of six geostationary satellites of the operational fleet: MTSAT-1, GOES-10/11/12, MSG-2 and METEOSAT-7, whose characteristics are summarized in Table 1. Depending upon the satellite under consideration, spatial resolution at nadir varies from 3 km for MSG-2 to 5 km for METEOSAT-7. Full disc data from the geostationary satellites are available from at least 15 min (MSG-2) to 3 h (GOES-11/12). The detection and tracking of MCSs (see next section) require a 30 min or better frequency for the infrared images. Such a requirement imposes the use of subsets of images scanned by the GOES-10/11/12 and MTSAT-1 platforms. Thus the South American region is scanned by GOES-10 every 15 min, while the North American region, the North Pacific region

Table 1. Technical characteristics of the operational geostationary satellite fleet and associated imagers used to process the entire intertropical belt for the monsoonal period in 2009.

Satellite	Satellite position	Full disc coverage	IR channel Imager	Spatial resolution	Time resolution	Tracking coverage	Lack data
Goes-10	60°W	None	10.7 μm I-M	4 km	30 min	108−36°W; 40°S−0°N	12%
Goes-11	135°W	3 h	10.7 μm I-M	4 km	30 min	180−108°W; 0−40°N	1.4%
Goes-12	75°W	3 h	10.7 μm I-M	4 km	30 min	108−W; 0−40°N	4.8%
MSG-2	0°	15 min	10.8 μm SEVIRI	3 km	15 min	36°W−36°E 40°S−40°N	0.5%
METEOSAT-7	57.5°E	30 min	11.5 μm MVIRI	5 km	30 min	36−108°E; 40°S−40°N	5.3%
MTSAT-1	140°E	1 h	10.8 μm JAMI	4 km	30 min	108−180°E; 0−40°N	2%

and the Chinese region are monitored by GOES-12, GOES-11 and MTSAT-1, respectively, with a 30 min frequency. The current acquisition mode of MTSAT-1 does not allow adequate sampling of the Southern Hemisphere region. Data transfer problems have also prevented us from accessing the archive of GOES-11 Southern Hemisphere at full temporal resolution. As a consequence, in this study MCSs are detected and tracked all over the tropical belt except for the Australian region and the South sector of GOES-12. A quality-control step (Szantai *et al.*, 2011) has been applied on time series on each geostationary data, and the percentage of missing images has been computed for the JJAS period in 2009 and reported in Table 1. Missing images are more frequent for GOES-10 (12%) and less frequent for MSG-2 (0.5%) but in any case the data availability remains good enough for our study.

2.2. Life cycle of MCS from geostationary IR observations

2.2.1. Algorithm description

The algorithm is based on previous efforts (Williams and Houze, 1987; Arnaud *et al.*, 1992; Mathon and Laurent, 2001) and is composed of two steps: the detection of convective cloud systems or convective clusters at a given time, and tracking along the time of the convective systems. The identification of convective clusters is performed by applying a cold brightness temperature threshold on each IR geostationary image in order to delineate contiguous regions in space colder than this threshold. A threshold of 233 K has been selected to stay in line with previous similar investigations (Duvel, 1989; Machado *et al.*, 1998; Roca and Ramanathan, 2000; Fiolleau *et al.*, 2009; Laing *et al.*, 2011) that showed that such a threshold was well adapted to the delineation of tropical MCSs and accumulated convective precipitation in the Tropics. Once all the IR images have been segmented, the tracking of convective systems is performed; only the cold clusters covering more than 5000 km² are considered further and smaller objects are disregarded by the tracking algorithm. Below this value, the tracking is indeed difficult to implement because of the cloud number, which increases strongly, while the overlapping area tends to be limited. Consequently, the number of split and merge artefacts increases artificially (Machado *et al.*, 1998). Clusters detected in the image at time $t + 1$ are matched with those in the previous image at time t based on the spatial overlap between the two segmented images. If the overlap is greater than 50% or 10 000 km² of the area of either the current cluster or the cluster from the previous image, the clusters are matched. Too weak a criterion will imply a difficulty in tracking MCSs with a

high propagation speed and will give rise to a large number of split artefacts. Conversely, too high an overlap criterion will imply more merge artefact events. Hence it appears that for a 30 min frequency dataset our overlap criterion can accommodate both the rapidly moving (15−30 m s^{-1}) (Machado *et al.*, 1998; Mathon and Laurent, 2001) squall lines and the slower non-squall clusters found in the tropical regions (Houze and Betts, 1981; Futyan and Del Genio, 2007).

When no overlapping occurs in the previous image, it is considered that the cloud system is generated. On the other hand, a convective system dissipates when there is no longer intersection with another cluster in the next image. Thus a convective system is defined as a succession of convective clusters, which have been segmented in successive images. The tracking can result in some clusters merging and splitting, yielding complex MCS life cycles. When several clusters merge to form a unique cluster in the next image, the larger cluster at this time is selected to continue the original track, whereas the tracks of the smaller clusters are considered to end. Similarly, splitting clusters are taken into account by selecting the larger cluster in the next image to continue the track and the smaller clusters are considered as split generation. For this study, a selection is applied to the MCS generated by a split, or dissipated by a merge, in order to keep convective systems describing a complete life cycle. Consider that the cluster B in the current image is generated by a split of cluster A in the previous image. If the lifetime of cluster B is longer than the lifetime of cluster A, from its genesis to the moment of its split, then cluster B is considered as having described a complete life cycle and is selected in our database. A similar process is applied for convective systems dissipated by a merge. This approach hence filters MCSs describing a complete life cycle. Overall, the rejected MCSs account for 32% of the whole population and 22% of the total cold cloudiness. Table 2 details the fraction of rejected MCSs for each geostationary platform. Missing images in the time series are handled as follows: if few images are missing, a recovery process is run to continue the track of each convective system during the period of missing images. This process is based on the generation of the missing images, by extrapolating the behaviour of each convective system (locations, cold cloud area). The maximum number of successive missing images has been set to 10 images, meaning a time series of 5 h (2 h 30 min) for a 30 min (15 min) geostationary temporal resolution.

Hence only a marginal amount of the systems artificially initiate or dissipate from a greater time series of missing images (6%). The tracking algorithm is applied independently on each geostationary satellite over the whole

Table 2. Contribution of rejected MCSs to the total population and to total cold cloudiness; and contribution of the three different MCS classes to the total population and to total cold cloudiness for the region covered by different geostationary satellite platforms.

		MSG-2	METEOSAT-7	MTSAT-1	GOES-10	GOES-11	GOES-12
Contribution of rejected MCS	Population	23%	35%	32%	21%	29%	27%
	Cold cloudiness	15%	27%	8%	17%	18%	14%
Contribution of Class 1	Population	52%	50%	52%	60%	49%	51%
	Cold cloudiness	5%	3%	4%	6%	4%	6%
Contribution of Class 2a	Population	17%	11%	12%	15%	16%	17%
	Cold cloudiness	69%	55%	68%	64%	62%	68%
Contribution of Class 2b	Population	4%	4%	4%	4%	6%	5%
	Cold cloudiness	11%	15%	21%	13%	16%	12%

2009 monsoonal summer period, providing segmented images and a database collecting the MCS morphological parameters. The very few MCSs for which the tracking was impacted by missing/bad-quality images have been removed from the statistics. The resulting morphological parameters of the MCSs include the area of the system (km^2), the mean IR brightness temperature (K) and the speed of propagation (m s^{-1}) as a function of time during the MCS life cycle. Integrated MCS parameters like the lifetime duration (h), MCS genesis and lysis date, cumulated area (km^2) and average speed of propagation (m s^{-1}) are also computed. The location of the systems is defined by the centre of mass weighted by the brightness temperature of each pixel within the cluster.

2.3. Life cycle of MCSs

Once the time series of the geostationary observations have been processed, two more treatments are performed to extract the relevant information. The first one consists of a simple classification of the MCS. The second uses a normalization technique to homogenize the life cycle of the whole population of systems.

2.3.1. Classification

The last two decades of analysis of IR geostationary imagery have yielded a large corpus of studies focused on the MCS, resulting in a large amount of definition and classes, from Maddox's (1980) subset of storms, the mesoscale convective complexes (MCC), convective cloud clusters (CCC), disorganized convective systems and tropical storms (e.g. Evans and Shemo, 1996) to the Sahelian Organized Cloud Systems (OCS) (Mathon and Laurent, 2001) and 'super-clusters' (Mapes and Houze, 1993). Most of these categorizations are based on various considerations related to the morphological parameters of the clusters forming the storm (minimum size, eccentricity, minimum duration, temperature, etc.). While these classifications have shown a strong potential to structure the analysis of the storms locally, i.e. for the region for which they were initially proposed, none of them is useful at the global scale. We have therefore adopted here a very simple classification scheme based on the cold cloud shield life cycle. This is discussed in detail in Fiolleau (2010). First, a 5 h threshold applied on the MCSs lifetime durations is used to split the entire population into two subsets: Class 1 for the MCSs lasting less than 5 h, and Class 2 for the others. The systems lasting more than 5 h are further analysed. The systems, for which a single, well-defined,

maximum size within the time evolution of the cold cloud shield is found, form Class 2a. The remaining systems, characterized by a more complex life cycle (multiple maxima, plateau, etc.), are attributed to Class 2b. In the following, only MCSs belonging to the Class 2a systems are further considered and analysed. The contribution to the whole population and to the total cold cloudiness of each MCS class is presented in Table 3. The contribution of the Class 2a systems to the total cold cloudiness varies between 55% and 70% according to the region of interest.

2.3.2. Discretization and normalization

In the perspective of the compositing step (section 3.2), and in line with previous compositing efforts (McNally and Cotton, 1989), the MCS life cycles belonging to Class 2a are normalized. The life cycle of each MCS is normalized between 0 and 100% and is further discretized into ten 10% stages. The size of the cold cloud shield is also normalized between 0 and 1 at its maximum. Hence all the system shield life cycles are made easily comparable (Roca and Fiolleau, 2013). Given the 30 min frequency requirements followed here for the tracking of the clouds, the life cycle of the systems lasting less than 5 h cannot be resolved with a 10% step. Consequently, the Class 1 systems life cycle is not analysed further.

2.3.3. Instantaneous retrievals from the TMI instrument on board the TRMM satellite

The BRAIN retrieval algorithm (Viltard et al., 2006) was originally derived from the GPROF algorithm (Kummerow et al., 2000). The technique is based on a Bayes/Monte Carlo scheme to retrieve a suite of rainfall information from a vector of measured multispectral microwave brightness temperatures obtained from a microwave imager. The most probable rain rate is computed from the weighted average of the possible rain rates stored in the retrieval database. The specifics of BRAIN lie in its retrieval database, which is exclusively made of co-located TMI and PR data. The advantages are the absence of errors due to radiative transfer simulation and a natural PDF of the rain events (as seen by the PR). It is important to note that BRAIN does not use any a priori information during the retrieval process, relying exclusively on the natural PDF of the measured rain and the error-free brightness temperatures stored in its retrieval database. BRAIN will provide Day 1 instantaneous rain estimates from the MADRAS radiometer for the Megha-Tropiques mission (Roca et al., 2010). The

Table 3. Contribution of class 2a MCSs to the total population and to total cold cloudiness for the regions covered by different geostationary satellite platforms.

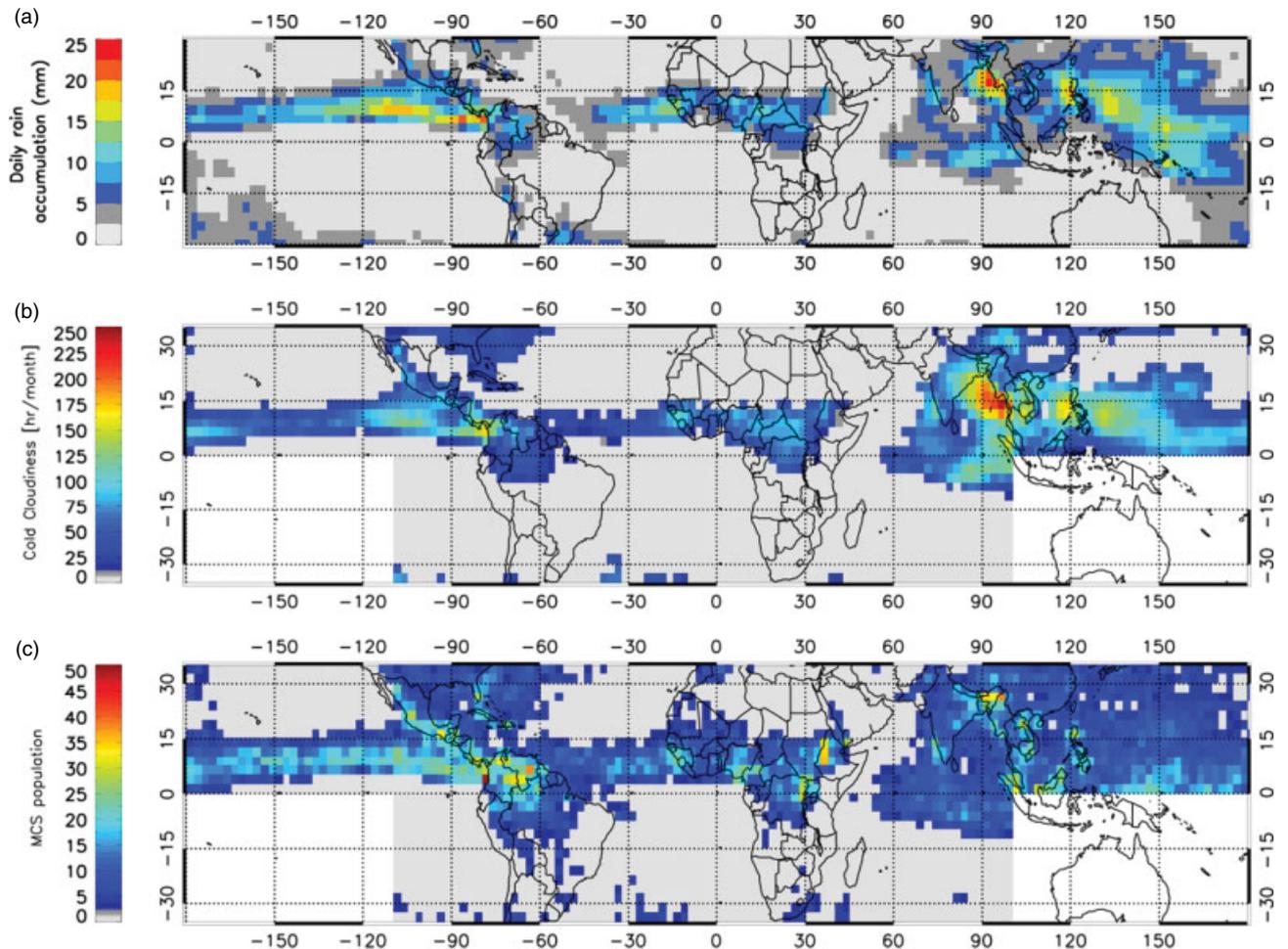|		MSG-2	METEOSAT-7	MTSAT-1	GOES-10	GOES-11	GOES-12
Contribution of Class 2a	Population	54%	56%	61%	44%	65%	64%
	Cold cloudiness	80%	69%	73%	64%	73%	76%

Figure 1. (a) Map of 2.5° TAPEER rain accumulation (Chambon *et al.*, 2012) for the monsoonal period. (b) Map of cold cloudiness expressed in hours per month for a 2.5° grid box. (c) Map of the MCS population. The white colour in (b) and (c) in the southern part of the Pacific Ocean and in the Australian region corresponds to the missing data.

uncertainty of these instantaneous rainfall estimates is described at length in Kirstetter *et al.* (2012) and when accumulated in Chambon *et al.* (2012a). In the present study, we use the BRAIN retrievals of the instantaneous surface rain rate derived from the TMI imager for the summer 2009 period over the whole intertropical belt. The convective area within a cloud cluster is identified using a threshold on the 85 GHz polarization corrected temperature (PCT). A threshold of 225 K is chosen to delineate the convective region of the cloud shield (Mohr and Zipser, 1996; Bouniol *et al.*, 2010). The convective rain fraction is then computed as the ratio of the convective rainfall surface divided by the total precipitation of the cold cloud shields.

2.4. Results for the 2009 summer season

The main features of the distribution of rainfall and MCSs for the summer season are presented in Figure 1.

Climatological features such as monsoon rain belts and the oceanic intertropical convergence zone (ITCZ) are well seen. The maximum amounts of rain are encountered over the Bay of Bengal and off the coast of Colombia, with values in excess of 20 mm per day. The correlation between the cold cloudiness (Figure 1(b)) with the accumulated rainfall map at the seasonal scale (Figure 1(a)) is, as expected, strong. Departures from the rainfall are indicative of local variations in the cloud-to-rain efficiency. For instance, off the coast of Colombia, cold cloudiness averages around 150−170 h per month and over the Bay of Bengal it reaches values up to 200−220 h per month, while rain accumulation is similar in the two regions. Figure 1(c) reports the occurrence of the MCSs. The preferred locations for MCSs are off the coast of Colombia and the Eastern Pacific ITCZ. The strong link between orography and MCS occurrence is also revealed, in particular for West Africa, with local maxima over the Guinean mountains, Mont Cameroon and the Ethiopian plateau. MCSs are also
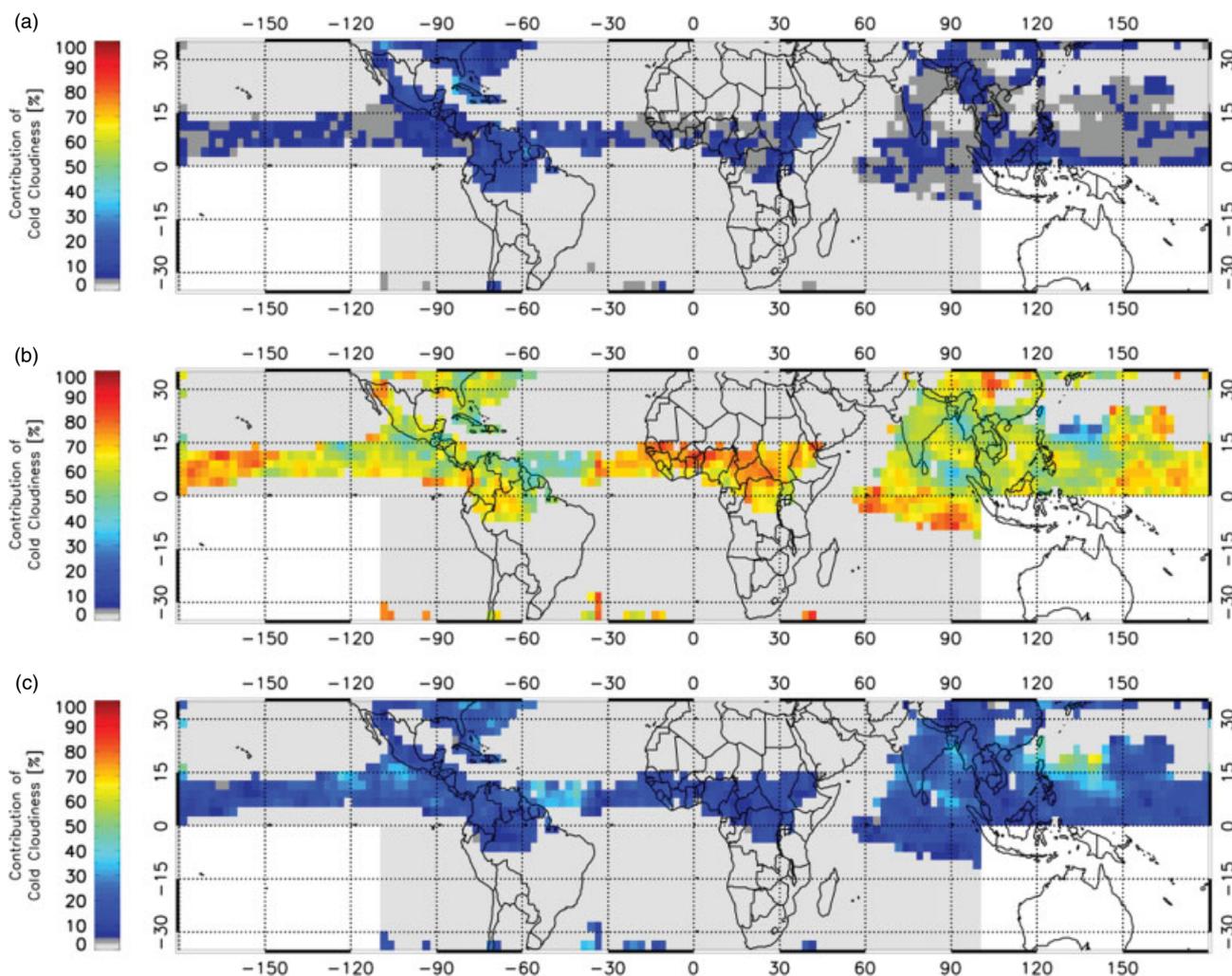
Figure 2. (a) Contribution of Class 1 MCSs to total cold cloudiness (%); (b) for Class 2a; (c) for Class 2b. The white colour in the southern part of the Pacific Ocean and in the Australian region corresponds to the missing data.

numerous over the Amazonian region. The same patterns are found in previous atlases of organized convective systems obtained either from local (Tomasini *et al.*, 2006; Fiolleau *et al.*, 2009) or global studies (Mohr and Zipser, 1996; Laing and Frisch, 1997; Liu *et al.*, 2007). No simple relationship emerges between the accumulated rainfall, cold cloudiness and MCS occurrence, which are all eventually linked via the precipitation life cycle of the storms. This supports the need for documenting these cycles and their regional variability in the Tropics. The relative contribution of the three classes of MCS to total cloudiness (Figure 2) reveals the overwhelming role of Class 2a as well as some regional exceptions. Class 1 systems generally do not contribute more than 20% to the total cloudiness and are mainly important over the American continent (Figure 2(a)). Class 2a frequently accounts for more than half of the total cold cloudiness, reaching more than 75% over wide areas such as the African continent region (Figure 2(b)). The contribution of Class 2b storms (Figure 2(c)) is evenly distributed and corresponds to roughly 20–25% of the cold cloudiness except in the Western Atlantic area and in the Bay of Bengal, where Class 2b can contribute up to 40%. Over the Western Pacific region, this contribution dominates, with values in excess of 70%.

3. Compositing low Earth-orbiting observations along the MCS life cycle

3.1. Sampling considerations and rationale for the composite approach

The ability of a suite of space-borne microwave observing systems to sample the life cycle of the tropical MCS is now investigated. Three sampling options have been selected to evaluate the impact of the forthcoming microwave imager's missions on the documentation of the life cycle of the tropical MCS. The first one is the reference case, involving the use of TMI on board the TRMM mission alone. The second involves the use of the Microwave Analysis and Detection of Rain and Atmospheric Structures (MADRAS) instrument on board the Megha-Tropiques (MT) mission alone. The last sampling configuration aims to mimic the microwave imaging fleet for the era of the Global Precipitation Mission (Hou *et al.*, 2008) and is composed of TMI on board TRMM, MADRAS on board MT, three MADRAS-like hypothetical instruments on board sun-synchronous satellites and the GPM-Core platform. The MT orbit as well as the MADRAS scanning geometry and the GPM-CORE platform have been simulated using IXION software (Capderou, 2009) and provide realistic observing conditions for our computations. Spatial and temporal samplings are to be considered. Note
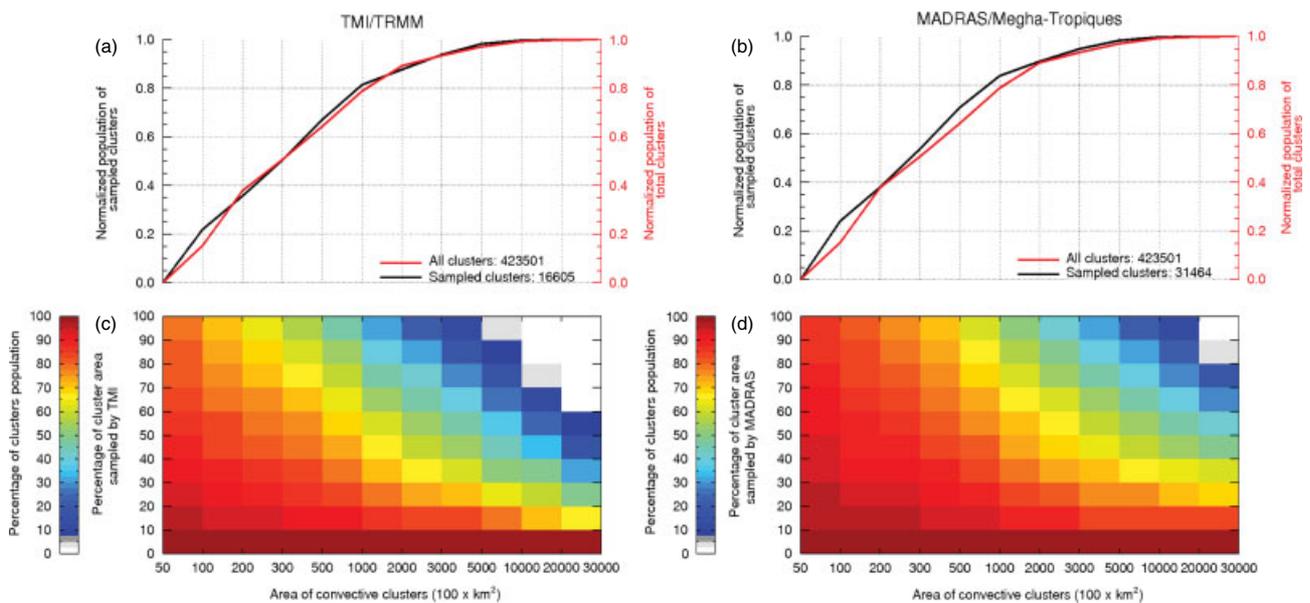
Figure 3. (a) Cumulated distribution function of the area of the total population of convective clusters (red line) and of the convective clusters sampled by the TMI instrument (black). (b) The same but for the Madras instrument. (c) 2D distribution of the convective cluster population sampled by TMI according to the area of convective clusters (km^2) and the percentage of cluster area sampled by the TMI instrument (%). (d) The same but for the MADRAS instrument (%). Each area interval corresponds to a cumulated distribution function and results are expressed as a percentage.

that we defer for future work investigation of the sensitivity of the results, for the constellation case, to the use and merging of retrievals from multiple platforms with various instrumental resolutions. With respect to spatial sampling, the limited widths of the swath of the microwave instruments have to be accounted for, as only a portion of individual convective clusters may be sensed by a radiometer, lowering its significance at the system scale. In particular, the larger the cluster, the lower is the probability of the cluster area being totally matched. Similarly, a small swath width of the microwave instrument yields difficulties in matching the entire area of convective cluster. The TMI sensor on board TRMM has a swath width of 878 km. Considering a typical cluster associated with its equivalent ellipse with an eccentricity equal to 0.7 (Maddox, 1980), TMI observations, in the best case, fully cover the convective cloud clusters up to roughly 860 000 km^2. The swath of 1741 km of the MADRAS instrument on board Megha-Tropiques yields, under the same conditions, a maximum area of 3.3×10^6 km^2. Figure 3(a) and (b) compare the sampling conditions of the IR clusters between TMI and MADRAS (which encompass any of the anticipated participants' swaths in the GPM constellation), for a realistic population of clusters for summer 2009 over all the tropical belt. Only a few convective clusters have a cold cloud area greater than 860 000 km^2 (0.7%) but they belong to MCS, contributing to around 11% of the total cold cloudiness. For the period of study and over the whole tropical region, the larger cold cloud area encountered for an MCS during its life cycle is 2.8×10^6 km^2 over the Bay of Bengal on 17 July 2009. The fraction of the IR cluster sampled by the microwave imager is important for the cluster scale analysis. The IR-delineated cluster size distribution indicates that clusters larger than 200 000 km^2 are not frequent ($\sim$10% of the cluster population) but account for up to 56% of the cold cloudiness. At the MCS level, around 10% of the MCSs, at least once in their life cycle, exhibit a cluster larger than 200 000 km^2. Clusters sampled by the TMI/TRMM sensor with a fraction greater than 70% account for 68%

of cases up to 200 000 km^2 and 27% beyond (Figure 3(c)). In the MADRAS case, the overlap conditions of 70% are realized for 75% of clusters up 500 000 km^2 and less than 36% beyond. For these very large clusters, the sampling is not as good (Figure 3(d)). It is then important to keep in mind that very large clusters, infrequent but nevertheless contributing to 26% of cold cloudiness, are not well sampled by the current microwave sensors. The results are in good agreement with Nessbit *et al.* (2006), who explored the precipitation features (PF) sampling (not the IR cluster) and showed that the limitation induced by the relatively narrow swath of TMI/TRMM does not compromise the statistical significance of the results.

Dynamical sampling of the life cycle of the MCS is the second important aspect of the analysis. Computations have been performed under the best-case scenario and no spatial sampling threshold is considered. The TMI, MADRAS and GPM constellation have matched overall 56%, 65% and 96% respectively of the total population of MCSs at least once during their life cycle. Figure 4 reveals that whatever the duration of the storms the TMI instrument on board TRMM, at best, samples twice a given MCS. The MADRAS results show up to six samples for MCSs lasting more than 10 h and two to three samples on average. The constellation case reveals that systems with a duration longer than 20 h can be observed up to 12 times. When the spatial sampling effects are factored in (e.g. rejecting clusters with a low observed fraction), the dynamical sampling results are even more parsimonious. These results indicate that only a marginal number of MCSs are actually well observed at various stages of their life cycle, making the documentation of the latter rather poor despite the large amount of data under consideration. One way to tackle the limiting effect of the dynamical/spatial sampling of MCS objects during their life cycle by the microwave imager's fleet is to form composite structures of this large amount of data. Such a composite approach makes it possible to document continuously the precipitation processes within the MCS throughout their life cycles.
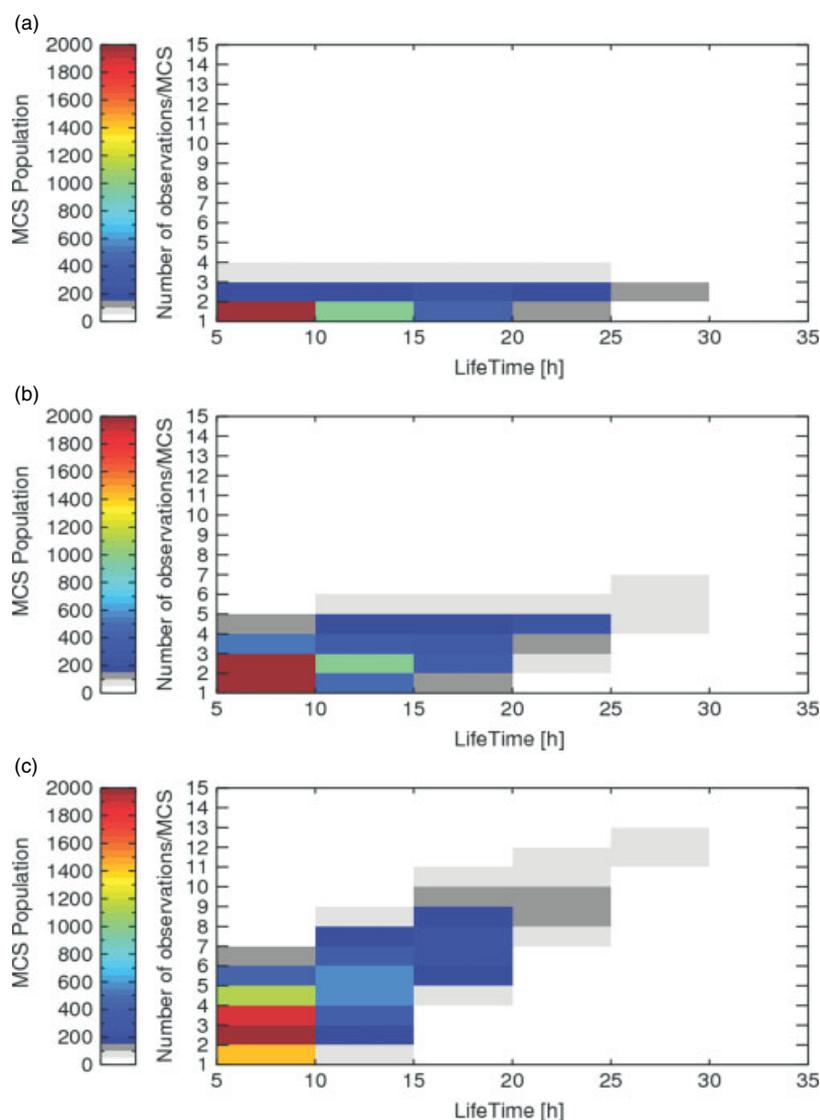
Figure 4. 2D distribution of MCS population according to their lifetime durations and average number of samples within the MCS life cycles (a) by the TMI instrument; (b) by the MADRAS instrument; (c) by the GPM constellation.

3.2. Composite of the low Earth-orbiting observations during the life cycle of the MCS

3.2.1. Collocation of geostationary and low Earth-orbiting observations

TMI observations are projected on to the closest geostationary IR slot using a time threshold of ± 15 min for a 30 min geostationary temporal acquisition scheme. Each BRAIN pixel (8 km resolution) is associated with the IR pixels using a nearest-neighbour approach. These data are further aggregated at the cluster scale, using the segmented images resulting from the tracking algorithm. System mean surface rain rates (mm h^{-1}), precipitating fraction (%) and convective rain fraction (%) are computed. A quality index is finally built by computing the fraction of the cluster that is covered with microwave data.

3.2.2. Composite of the life cycle

Clusters that have been coincidently observed by TMI and that have gone through the quality control procedure

are further composited within the ten 10% stages of the discretized life cycle following the technique of Cotton *et al.* (1989). As a result, a continuous view of the rain-related parameters, obtained from the low Earth-orbiting satellite, is available all through the life cycle of the MCS composite. As discussed in the next section, the robustness of the composite is sensitive to the number of observations in each life cycle stage. More information on the programming structure of the algorithm is available in Fiolleau *et al.* (2012).

3.2.3. Results for summer 2009

Figure 5 shows a composite resulting from the use of BRAIN data derived from the TMI radiometer on board the TRMM satellite during summer 2009 for both oceanic and continental conditions. Around 1000 clusters have been used to build each step of the composite (Figure 9(a)). The life cycle of the size of cold cloud shield is very similar between the two types of MCS and is characterized by a growing and a decaying phase almost symmetrical with respect to the life cycle (Fiolleau, 2010). The cluster mean rain rate varies from 6 to 2.5 mm h^{-1} from the beginning to the lysis of the continental storms and is significantly
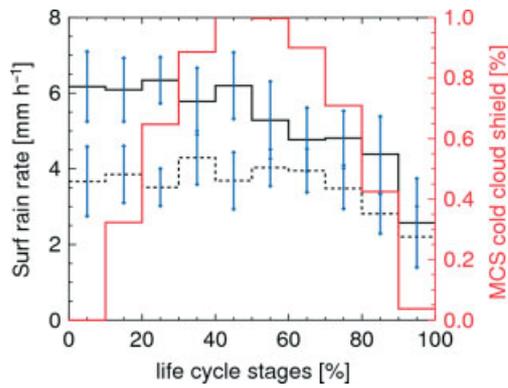
Figure 5. Evolution of the conditional average surface rain rate associated with continental (solid line) and oceanic (dashed line) convective systems over the entire tropical belt for the JJAS period in 2009. The blue lines correspond to the standard deviations for each step of the normalized life cycle. The red line represents the average evolution of the cold cloud shield associated with the MCSs.
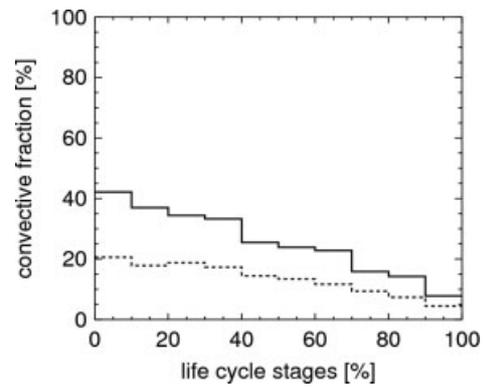

Figure 7. Evolution of the convective rain fraction as a function of the life cycle for continental (solid line) and oceanic (dashed line) systems over the entire tropical belt for the JJAS period in 2009. The convective rain fraction is computed as the ratio between the total precipitation for a PCT surface area lower than 225 K and the total precipitation of the convective cluster. See text for details of the computations.

smaller over the ocean (3.5–1.5 mm h^{-1}). The life cycle is composed of a first phase showing a steady rain rate during the anvil clouds (as depicted by the cold cluster) growth, followed by a smoothly decreasing phase while the anvil size shrinks. This life cycle is less marked for oceanic conditions than for the continental systems.

In order to better understand the differences between the land and oceanic regimes over the entire tropical regions, the distribution of the rain rate within the systems is investigated. Figure 6 indicates that indeed the small rain rates ($r < 3$ mm h^{-1}) are hardly contributing to the continental MCS rainfall, whereas they are a significant part of the oceanic systems. Thus, at the beginning of the life cycle, the precipitating fraction for rain rate greater than 0 mm h^{-1} is around 60% for oceanic conditions, whereas it is around 30% for the continental systems. The differences of precipitation intensities and precipitating fraction between oceanic and continental systems can be related to the difference in cluster precipitating fractions between the oceanic and continental clusters and are in line with previous regional studies of Futyan and Del Genio (2007) and of Kondo *et al.* (2006). Analysis of the convective fraction (Figure 7) confirms the diagnostic, with twice as much convective rain in the continental systems as in their oceanic counterparts. Note also the strong resemblance between the oceanic and land systems. In both cases –land and ocean –the convective fraction shows a very robust evolution during the life cycle of the MCS.

These results do not seem likely to be due to a land/sea artefact of the BRAIN algorithm, as a similar conclusion is drawn when the GPROF/2A12 official TRMM product is used instead (Fiolleau, 2010). The relevance of the composite precipitation life cycle of the MCS is dependent upon the representativity of the population of coincidently observed clusters at each stage of the life cycle to the whole MCS population. The microwave-observed fraction of the IR cluster is also an important factor governing the relevance of the estimation of the cluster mean parameters. The scale down to which such a compositing approach is able to provide insights into storm dynamics also deserves further scrutiny. All of these key aspects rely on details of the sampling of storms by the microwave imagery, which is investigated next.

4. Sensitivity to sampling by microwave imagery

4.1. Entire Tropics considerations

During summer 2009, over the entire Tropics more than 419 004 clusters have been detected, corresponding to 18 193 individual systems using IR imagery. Their spatial distribution (Figure 8(a)) closely resembles the map of the 2a MCS cold cloudiness (Figure 1(a)) with coincident extrema, in particular over the West African, Indian and Amazonian regions. Around 16 518 clusters (corresponding to 10 209 systems) were simultaneously observed by the TMI instrument, accounting for a quality index of 70%. These
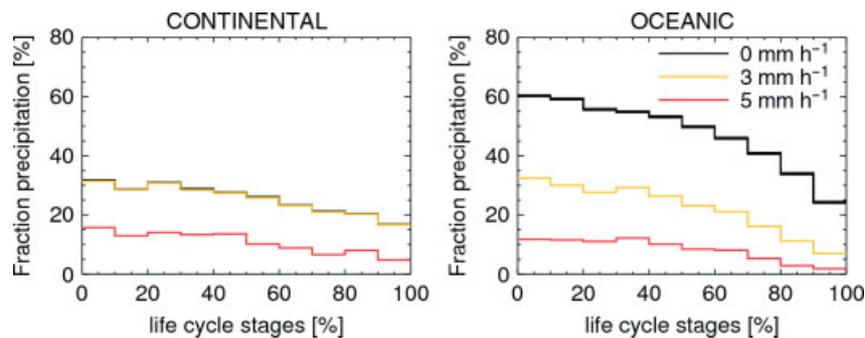

Figure 6. Evolution of the cluster area fraction precipitating more than a given threshold as a function of the MCS life cycle for the continental (left) and oceanic (right) systems over the entire tropical belt for the JJAS period in 2009.
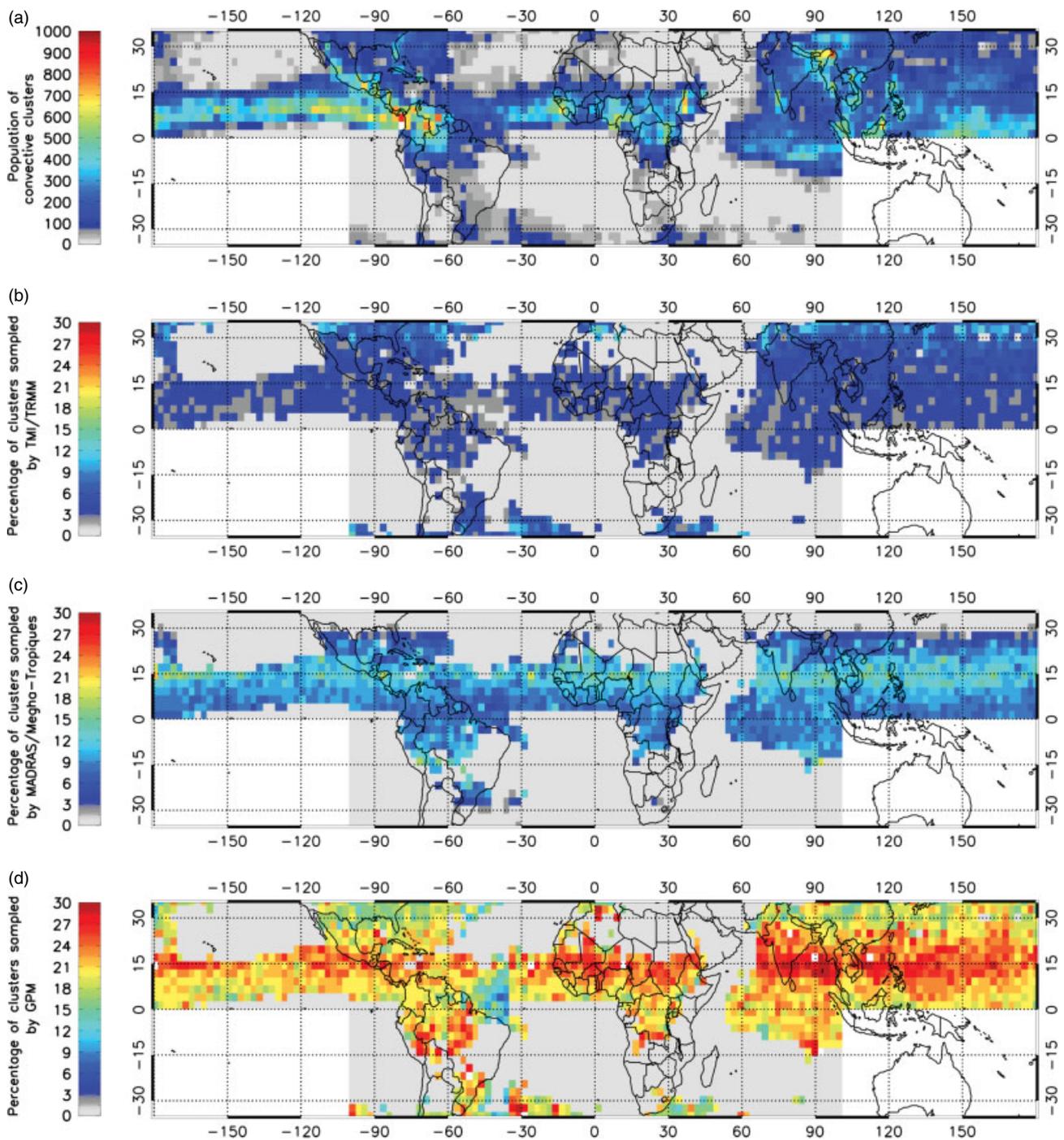
Figure 8. (a) Convective cluster population segmented by the tracking algorithm over the Tropics for the 2009 monsoonal period for a 2.5° grid box. Spatial distribution of the percentage of convective clusters sampled (b) by TMI/TRMM expressed as a percentage; (c) by MADRAS/Megha-Tropiques; (d) by the GPM constellation.

clusters are homogeneously distributed over the tropical belt, with slightly more frequent sampling around 32°N and 32°S latitude due to the inclination and height of the TRMM satellite (5% of the original local cluster distribution) (Figure 8(b)). This subset of clusters samples the life cycle evenly, with an average of 1650 cases per stage (Figure 9(a)). In the case of the MADRAS instrument (Figure 8c), more than 31 290 clusters are sampled during the same period, corresponding to 8–11% of the original cluster population. The consequence of the Megha-Tropiques orbit for the sampling by MADRAS is obvious with the significantly enhanced region between 12° and 15°, each side of the

Equator (Capderou, 2009; Roca *et al.*, 2010; Chambon *et al.*, 2012b). Again, an even sampling distribution is found along the life cycle with roughly between 2300 and 3200 samples per stage, depending upon the quality index (Figure 9(b)). Finally, for the constellation configuration, up to 20% of the IR clusters are sampled (more than 90 000). While the geographical distribution is rather uniform, one can nevertheless perceive the impact of MADRAS/MT on the constellation sampling results. Around 34% of the clusters observed by the constellation are indeed sampled by this instrument (Figure 8(d)). The constellation allows around 6000 samples per life cycle stage (at a medium quality index of
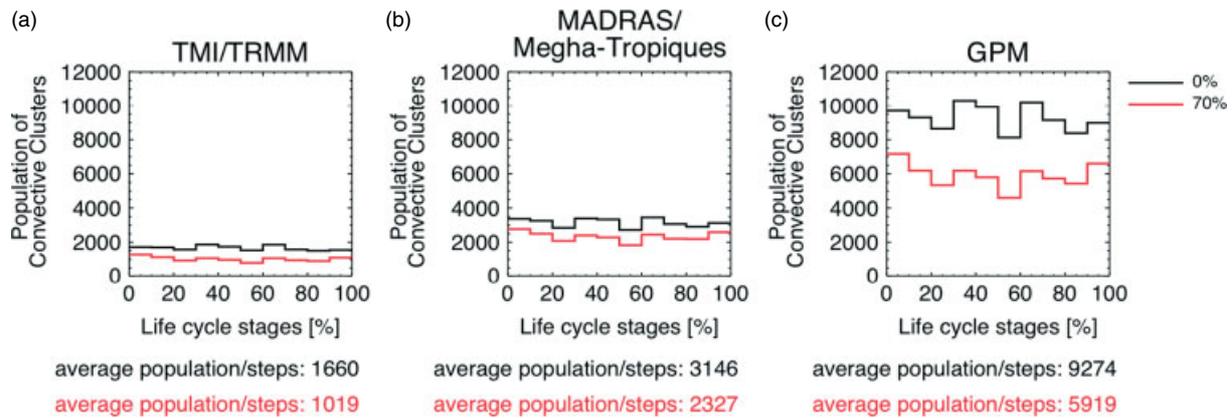
(a) (b) MADRAS/ (c)
Megha-Tropiques

Figure 9. Population of convective clusters sampled (a) by TMI/TRMM; (b) by MADRAS/Megha-Tropiques; (c) by the GPM constellation (right) for each step of the normalized life cycle, with no overlap condition (black) and with a 70% overlap condition (red).
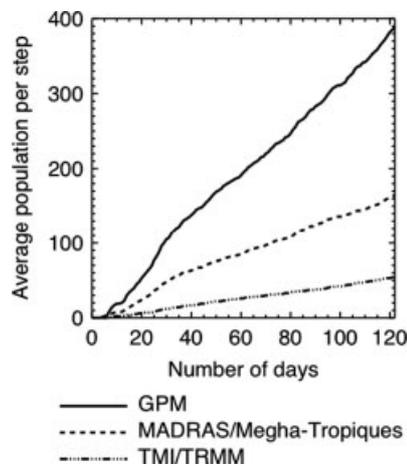

Figure 10. Distribution of the average convective cluster population sampled by TMI, MADRAS and GPM instruments for one stage of the MCS normalized life cycle, and according to the number of days processed. This figure is realized for MCSs which occurred over the Bay of Bengal.

70%) for the whole period and region under considerations. Figure 9 illustrates the subset of cluster population fulfilling this criterion for each step of the composite life cycle. On average, 60%, 73% and 64% of the convective clusters fulfil the 70% criteria along the composite normalized cycle for the TMI, MADRAS and GPM constellation respectively.

4.2. Regional considerations

Investigation of the dependence of MCS morphology and internal dynamics on its large-scale environment requires contrasting the precipitation life cycle over various large-scale regimes, which can be achieved through the construction of composite cycles at regional scales. Such an endeavour relies on the number of observations available for each stage of the life cycle. Tests indicated that a reasonable value of a minimum of 50 samples for each life cycle stage ensures statistical robustness. Considering the Bay of Bengal region ($65-100°$E, $10-30°$N), and using a criterion of 70% overlap between the IR cluster and the microwave imager, this minimum value of 50 samples is obtained: after 4 months for TMI/TRMM, 1 month for MADRAS/MT and only 3 weeks for the GPM constellation (Figure 10). Figure 10 further reveals that the constellation configuration overall permits sampling, at each life cycle stage, almost twice as

fast as the use of MADRAS/MT alone. Such a configuration opens the possibility of exploring composite life cycle at the intraseasonal scale (active/break phase of the monsoon; Madeen Julian Oscillation, etc.), which is difficult using a single observing system.

5. Conclusion and perspectives

A compositing method is presented that relates the morphological characteristics of tropical MCSs obtained from geostationary infrared imagery and a detection and tracking algorithm to the parameters derived from microwave imagers on board low Earth-orbiting satellites. The technique is illustrated on a representative subset of the population of the MCS over the tropical area during the boreal summer 2009 period. The composite life cycle of rainfall derived from the TMI radiometer on board the TRMM satellite is built as an example. This is the first composite build, for land and ocean, at the entire tropical belt scale. In both cases, rainfall is stronger during the early stages of MCS development and then decreases gradually as the MCS dissipates. Larger rain yields are observed for the land systems ($\sim$6 mm h^{-1} maximum) compared to systems over the ocean ($\sim$4 mm h^{-1} maximum). This confirms, at this Tropics-wide scale, the results of previous similar regional analyses (Kondo *et al.*, 2006; Futyan and Del Genio, 2007; Inoue *et al.*, 2009). The well-marked contrast during the evolution of the rainfall distribution as the MCS develops, matures and fades, between the land and oceanic conditions appears as a strong constraint to ongoing modelling efforts to represent organized convection and its effect upon the atmosphere for large-domain cloud-resolving models up to global climate model parametrizations. The sampling study further indicates that the use of a single observing system in low equatorial orbit, like Megha-Tropiques, improves upon an existing single platform like TRMM, but is outpaced when the whole constellation of microwave imagers is taken into consideration. The present results are indeed strongly encouraging us to take benefit from the Global Precipitation Mesourements missions' numerous microwave imagers and sounders (Hou *et al.*, 2008) to improve our documentation of the precipitation processes during the life cycle of the tropical MCS, provided a satisfactory solution to the complex issue of merging multiple-resolution radiometers is established. Beyond rainfall, it is anticipated that this technique could easily afford the building of the MCS life

cycle of some microphysical cloud top characteristics from the higher-frequency channels of the microwave imagers. It is also anticipated to extend the vertical description of the cloud system using the sounding capability of active instruments like the TRMM Precipitation Radata and Cloudsat radar (e.g. Cetrone and Houze, 2009) in time throughout the MCS life cycle. In the framework of the Megha-Tropiques mission, this algorithm has been prepared for operational exploitation at the French data-processing centre ICARE. The fleet of meteorological geostationary observations is continuously updated with the help of the French Service d'Archivage et de Traitement Météorologique des Observations Satellitaires. It will benefit from a systematic quality control of Level 1 geostationary IR observations (Szantai *et al.*, 2011). Various regions have been identified for building the composites using the outcome of the BRAIN algorithm run on the MADRAS instrument. The extension of such an approach to the Earth radiation budget parameters (outgoing long-wave radiation, top of atmosphere albedo) has also been anticipated where the instantaneous flux retrievals from the ScaRaB instrument (Viollier *et al.*, 2009) are used in the composite approach, as discussed in the technical documentation of the product (Fiolleau *et al.*, 2012). In the future, an updated version of the operational product is anticipated, in which the current tracking algorithm will be replaced with a new approach (Fiolleau, 2010; Fiolleau and Roca, 2013) that will, principally, increase the number of systems satisfying the requirements for the composite and hence facilitating the building of composites at smaller regional scales. Efforts towards making use of radiometers of various resolution in the rainfall retrievals are also being undertaken to eventually facilitate the use of the GPM constellation in the analysis of the life cycle of the MCS over the Tropics.

Acknowledgements

References

Arnaud Y, Desbois M, Maizi J, 1992. Automatic tracking and characterization of African convective systems on meteosat pictures. *J. Appl. Meteorol.* **31**: 443–453.

Boer E, Ramanathan V. 1997. Lagrangian approach for deriving cloud characteristics from satellite observations and its implications to cloud parameterization. *J. Geophys. Res.* **102**(D17): 21383–21399.

Bouniol D, Delanoë J, Duroure C, Protat A, Giraud V, Penide G. 2010. Microphysical characterisation of West African MCS anvils. *Q. J. R. Meteorol. Soc.* **136**: 323–344.

Capderou M. 2009. Megha-tropiques: sampling and comparison with other meteorological satellite. *Megha-Tropiques Technical Memorandum No. 3*. Available from http://megha-tropiques.ipsl.polytechnique.fr

Cetrone J, Houze RA Jr. 2009. Anvil clouds of tropical mesoscale convective systems in monsoon regions. *Q. J. R. Meteorol. Soc.* **135**: 305–317.

Chambon P, Jobard I, Roca R, Viltard N. 2012a. An investigation of the error budget of tropical rainfall accumulation derived from merged passive microwave and infrared satellite measurements. *Q. J. R. Meteorol. Soc.* DOI:10.1002/qj.1907.

Chambon P, Roca R, Jobard I, Capderou M. 2012b. The sensitivity of tropical rainfall estimation from satellite to the configuration of the microwave imagers constellation. *Geosci. Remote Sens. Lett. IEEE* **PP**: 1–5.

Cotton WR, Lin M-S, McAnelly RL, Tremback CJ. 1989. A composite model of mesoscale convective complexes. *Mon. Weather Rev.* **117**: 765–783.

Del Genio AD. 2012. Representing the sensitivity of convective cloud systems to tropospheric humidity in general circulation models. *Surv. Geophys.* **33**: 637–656.

Diongue A, Lafore J-Ph, Redelsperger JL, Roca R. 2002. Simulation at cloud and synoptic scales of the whole life cycle of a west African squall-line observed during HAPEX-Sahel: validation and scales interactions, *Q. J. R. Meteorol. Soc.* **128**: 1899–1928.

Duvel JP. 1989. Convection over tropical Africa and the Atlantic Ocean during northern summer. Part I: Interannual and diurnal variations. *Mon. Weather Rev.* **117**: 2782–2799.

Evans JL, Shemo RE. 1996. A procedure for automated satellite-based identification and climatology development of various classes of organized convection. *J. Appl. Meteorol.* **35**: 638–652.

Fiolleau T. 2010. Cycle de vie des systèmes convectifs de mousson dans les régions tropicales: préparation à la mission Megha-Tropiques, Thèse de doctorat de l'école polytechnique.

Fiolleau T, Roca R. 2013. An algorithm for the detection and tracking of tropical mesoscale convective systems using infrared images from geostationary satellite. *IEEE Transactions on Geoscience and Remote Sensing*, DOI: 10.1109/TGRS.2012.2227762.

Fiolleau T, Tomasini M, Roca R, Lafore J-P, Laurent H, Lebel T, Piriou C, Ramage K. 2009. Climatology of mesoscale convective systems from satellite. *AMMAEU report*, D.2.1.C.g. http://www.amma-eu.org/

Fiolleau T, Roca R, Aublanc J, Chomette O, Raberanto P, Gif N. 2012. Composite of convective systems: a Megha-Tropiques product. *Megha-Tropiques Technical Memorandum No. 5*. http://megha-tropiques.ipsl.polytechnique.fr

Futyan and Del Genio. 2007. Deep convective system evolution over Africa and the tropical Atlantic. *J. Climate* **20**: 5041–5060.

Grandpeix J-Y, Lafore J-P. 2010. A density current parameterization coupled with Emanuel's convection scheme. Part I: The models. *J. Atmos. Sci.* **67**: 881–897.

Hou AY, Skofronick-Jackson G, Kummerow C, Shepherd JM. 2008. Global precipitation measurement. In *Precipitation: Advances in Measurement, Estimation and Prediction*, Michaelides M (ed.). Springer: Berlin; 540pp, March 2008, ISBN: 978-3-540-77654-3.

Houze RA Jr. 1982. Cloud clusters and large-scale vertical motions in the tropics. *J. Meteorol. Soc. Jpn* **60**: 396–410.

Houze RA. 2004. Mesoscale convective systems. *Rev. Geophys.* **42**: 8755–1209.

Houze RA, Betts AK. 1981. Convection in GATE. *Rev. Geophys. Space Phys.* **19**: 541–576.

Inoue T, Vila D, Rajendran K, Hamada A, Wu X, Machado LAT. 2009. Life cycle of deep convective systems over the eastern tropical Pacific observed by TRMM and GOES-W. *J. Meteorol. Soc. Jpn* **87A**: 381–391.

Kirstetter P-E, Viltard N, Gosset M. 2012. An error model for instantaneous satellite rainfall estimates: evaluation of BRAIN-TMI over West Africa. *Q. J. R. Meteorol. Soc.* DOI:10.1002/qj.1964.

Kondo Y, Higuchi A, Nakamura K. 2006. Small-scale cloud activity over the maritime continent and the western Pacific as revealed by satellite data. *Mon. Weather Rev.* **134**: 1581–1599.

Kummerow C, Simpson J, Thiele O, Barnes W, Chang ATC, Stocker E, Adler RF, Hou A, Kakar R, Wentz F, Ashcroft P, Kozu T, Hong Y, Okamoto K, Iguchi T, Kuroiwa H, Im E, Haddad Z, Huffman G, Ferrier B, Olson WS, Zipser E, Smith EA, Wilheit TT, North G, Krishnamurti T, Nakamura K. 2000. The status of the Tropical Rainfall Measuring Mission (TRMM) after two years in orbit. *J. Appl. Meteorol.* **39**: 1965–1982.

Laing AG, Fritsch JM. 1997. The global population of mesoscale convective complexes. *Q. J. R. Meteorol. Soc.* **123**: 389–405.

Laing AG, Carbone RE, Levizzani V. 2011. Cycles and propagation of deep convection over equatorial Africa. *Mon. Weather Rev.* **139**: 2832–2853.

Liu C, Zipser EJ, Nesbitt SW. 2007. Global distribution of tropical deep convection: differences using infrared and radar as the primary data source. *J. Climate* **20**: 489–503.

Machado LAT, Laurent H. 2004. The convective system area expansion over Amazonia and its relationships with convective system life duration and high-level wind divergence. *Mon. Weather Rev.* **132**: 714–725.

Machado LAT, Rossow WB, Guedes RL, Walker AW. 1998. Life cycle variations of mesoscale convective systems over the Americas. *Mon. Weather Rev*. **126**: 1630–1654.

Maddox RA. 1980. Mesoscale convective complexes. *Bull.Am. Meteorol. Soc*. **61**: 1374–1387.

Mapes BE, Houze RA. 1993. Cloud clusters and superclusters over the oceanic warm pool. *Mon. Weather Rev*. **121**: 1398–1416.

Mathon V, Laurent H. 2001. Life cycle of Sahelian mesoscale convective cloud systems. *Q. J. R. Meteorol. Soc*. **72**: 105–110.

McAnelly RL, Cotton WR. 1989. The precipitation life cycle of mesoscale convective complexes over the central United States. *Mon. Weather Rev*. **117**: 784–808.

Mohr KI, Zipser EJ. 1996. Defining mesoscale convective systems by their 85 GHz ice-scattering signatures. *Bull. Am. Meteorol. Soc*. **77**: 1179–1189.

Nesbitt SW, Cifelli R, Rutledge SA. 2006. Storm morphology and rainfall characteristics of TRMM precipitation features. *Mon. Weather Rev*. **134**: 2702–2721.

Pritchard MS, Moncrieff MW, Somerville RCJ. 2011. Orogenic propagating precipitation systems over the United States in a global climate model with embedded explicit convection. *J. Atmos. Sci*. **68**: 1821–1840.

Roca R, Fiolleau T. 2013. The life cycle of monsoonal convective systems cloud shield over West Africa, India and the Adjacent Oceans as seen from METEOSAT observations. *Mon. Weather Rep*. (in preparation).

Roca R, Ramanathan V. 2000. Scale dependence of monsoonal convective systems over the Indian Ocean. *J. Climate* **13**: 1286–1298.

Roca R, Berges JC, Brogniez H, Capderou M, Chambon P, Chomette O, Cloche S, Fiolleau T, Jobard I, Lemond J, Ly M, Picon L, Raberanto P, Szantai A, Viollier M. 2010. On the water and energy cycles in the Tropics. *CR Geosci* **342**: 390–402.

Szantai A, Six B, Cloché S, Sèze G. 2011. Quality of geostationary satellite images. *Megha-Tropiques Technical Memorandum No. 3*. http://meghatropiques.ipsl.polytechnique.fr

Tomasini M, Lafore J-P, Piriou C, Roca R, Ramage K, Laurent H, Morel C, Senesi S. 2006. Atlas on a climatology of West African mesoscale convective systems. *AMMA-EU report* Du2.1.3.a. http://www.amma-eu.org/

Viltard N, Burlaud C, Kummerow CD. 2006. Rain retrieval from TMI brightness temperature measurements using a TRMM PR-based database. *J. Appl. Meteor. Climatol*. **45**: 455–466.

Viollier M, Standfuss C, Chomette O, Quesney A. 2009. Top-of-atmosphere radiance-to-flux conversion in the SW domain for the ScaRaB-3 instrument on Megha-Tropiques. *J. Atmos. Oceanic Technol*. **26**: 2161–2171.

Williams M, Houze RA. 1987. Satellite-observed characteristics of winter monsoon cloud clusters. *Mon. Weather Rev*. **115**: 505–519.

Yuan J, Houze RA Jr. 2010. Global variability of mesoscale convective system anvil structure from A-train satellite data. *J. Climate* **23**: 5864–5888.

Yuter SE, Houze RA Jr. 1998. The natural variability of precipitating clouds over the western Pacific warm pool. *Q. J. R. Meteorol. Soc*. **124**: 53–99.